Astronomical and Astrophysical Transactions (*AApTr*), 2023, Vol. 33, Issue 4, pp. 411–436,
ISSN 1055-6796, Photocopying permitted by license only, ©Cambridge Scientific Publishers

A simulation of the RAMSES project and a study of the effect of the number of used telescopes on the time required for the observation of transient astrophysical event

A. Gueboudji, S. Aoudia*

Laboratoire de Physique Théorique, Faculté des Sciences Exactes, Université de Bejaia, Bejaia, 06000 Algeria

Received 15 February, 2022; in revised form 30 July 2022

National Aures Observatory is an observatory under construction, which consists of a network of 12 to 16 small robotic telescopes associated with a large telescope (of 1 or 2 m) equipped with a spectrometer. Its first interests will be multi-messenger astronomy and tracking of the optical counterpart of gravitational waves. In this work, we optimized the use of this network by using the branch and bound optimization method. In addition we also studied the effect of the number of used telescopes on the time required for an observation. This was done by analyzing how the number of used telescopes affects the probability of observing, each time the telescopes are re-pointed. Thus, we could build a strategy allowing us to know the number of telescopes needed for an observation knowing the size of the area to be surveyed. Accordingly we were able to reduce the time required to observe an astronomical event in a sky position error area of about 100°^2} with the use of a network of 6 telescopes to only about a minute. Moreover, we found that by using the whole network of 12 telescopes, 42.04% of the simulation runs were able to observe the event in the first pointing to the error area.

Keywords: Multi-messenger, gravitational waves, gamma ray bursts, RAMSES Project, National Aures Observatory, branch and bound method, TAROT telescope

1 Introduction

Gravitational waves (GW) were first detected by the two detectors of LIGO (Hanford, WA, and Livingston, LA) simultaneously on September 14, 2015 (Aasi et al. 2015; Abbott et al. 2016) which represents an experimental verification of what the theory of general relativity came up with a century ago. About two years later, on August 17, 2017, a gravitational wave signal was detected by Virgo and LIGO (Abbott et

*Email: sofiane.aoudia@univ-bejaia.dz

al. 2017), and a few seconds later, a gamma ray burst (GRB) signal was detected from the same source (Abbott et al. 2017), heralding a new era in astrophysics, meaning multi-messenger astrophysics (MMA). The use of the MMA will enable us to solve major problems in the field of GW astronomy. More precisely, it will allow a much better localization of the GW sources (estimated to 100°^2}, at best, with a GW detection alone (Camp et al. 2013)).

Small telescopes, like TAROT (Télescope à action rapide pour les objets transitoires, "Rapid-action telescope for transient objects") (Klotz et al. 2009), play a very important role in following up and localizing these transient phenomena because they are usually very fast and robotic, which makes them quick to respond and highly effective. In this regard, the implementation of the Robotic Advanced Multimessenger and Space Environment Surveyor (RAMSES) project was chosen by a team of specialists (Seghouani and Boër et al) (Seghouani et al. 2019) at the National Aures Observatory (NAO), which is an association of a network of telescopes of up to 16 very fast robotic telescopes of the TAROT type and a large telescope equipped with a spectrometer, whose main objectives will be multi-messenger astronomy and the observation of optical counterparts of GWs and GRBs, as well as some secondary objectives such as the early supernovae search and tracking of asteroids, variable stars, and exoplanets.

In this research paper, which represents a simulation of this observatory (where some of its main features are given in detail in Section 4), we will see how to exploit it optimally and achieve its primary and secondary objectives completely and consistently, by studying the effect of the number of telescopes on the time needed to observe the astronomical phenomenon and the effectiveness of telescopes in finding the source every time they are redirected.

This simulation programming is based on an optimization method, called branch and bound (BB) technique, which solves the assignment problem that simulates the process of pointing each telescope to a given place to be scanned. The simulation steps are detailed in Section 5. We get interesting results that we will show and discuss in Section 6.

2 Gravitational waves

The notion of GW appears in scientific literature as early as 1900 with Lorentz who imagined a gravitational field to propagate (Lorentz 1899). In 1905, Poincaré introduced the concept of a "gravity wave" (Poincaré 1905). Although, he defined waves that do not carry energy and his concept already conveys the idea that these waves travel at the speed of light.

It was not until 1916 that Einstein theoretically predicted the existence of GWs by presenting them as solutions of his equations (Einstein et al. 1905). To reach this conclusion, Einstein considered a perturbation of flat space-time, thus linearizing his equations.

The nature of GWs was first determined in the early 1950s. Pirani showed the relationship between the Riemann tensor and the strain of the metric (Pirani 1956). Considerations on the perturbation of a flat space-time become a special case of GW theory. Unlike other aspects of general relativity, the experimental validation of

Einstein's predictions about the existence of GWs took many years. the binary pulsar PSR1913+16 provided indirect evidence for the existence of gravitational radiation. But it wasn't until 100 years after Einstein's work that the first direct detection of GWs was made in LIGO detector data in 2015, putting an end to all controversies over their existence for good. (Aasi et al. 2015) Then, on August 17, 2017, Virgo and LIGO detected a gravitational wave (GW170817), and two seconds later, a gamma-ray burst GRB170817A was detected, resulting from the merger of two neutron stars by Fermi-GBM in the same region. This was a scientific achievement with far-reaching prospects in improving the estimation of the GW source parameters. One of the most important problems in this field is, in fact, to improve the estimation of the source localization of the astrophysical phenomenon, which using the initial operating phase of the GW network observatories alone, reaches 100 square degrees (Camp et al. 2013), which is very large. The solution to this problem lies in the combination of GW and electromagnetic (EM) data, in the so-called multi-messenger astronomy.

Multi-messenger astronomy MMA is astronomy that relies on the recording and interpretation of various signals from the same region of the space (Rollins 2011). The four messenger signals are gravitational waves, electromagnetic radiation, cosmic radiation, and particles, including neutrinos, as well as electrons, protons, etc, which are generated by various astrophysical processes (Branchesi 2016), and allow us to obtain various information about the sources in which they occur. The most famous event that is a gateway to multi-messenger astronomy is the GW170817, a source with over 4000 Messengers (Beckman 2021). The GRB 170817A gamma-ray burst was observed by the Fermi Gamma-ray Space Telescope and INTEGRALE, and its optical counterpart SSS17a was detected 11 hours later in the host galaxy NGC4993 at the Las Campanas Observatory (Coulter et al. 2017). This observation was supplemented by other observations in optics by the Hubble Space Telescope and the Dark Energy Survey, in ultraviolet rays by the Swift Gamma-Ray Burst Mission, in X-rays by the Chandra X-ray Observatory and in radio waves by the Karl G. Jansky very large array (VLA) (Beckman 2021).

Gravitational wave sources The most compact known stars are neutron stars and black holes. Cataclysmic phenomena including these compact objects can be of several types, and they can be classified into three families (Frey 2018):

1. Transient sources lasting from a few milliseconds to a few seconds, such as the collapse of a star's core at the end of its life or the fusion of black holes.
2. Continuous and stable sources over the observation time scale. For example, the stochastic background is the accumulation of all emissions since the beginning of the Universe or pulsars.
3. Long-term transient sources range from a few tens of seconds to several minutes.

In this paper, we are particularly interested in long-term transient sources because the RAMSES project telescopes have a slewing time of about 1.5 seconds, and the alert (eg: from Swift-GCN) takes about 20 seconds. Only long-term transient sources can be studied with this network of telescopes during the prompt phase.

Long-term transient sources For most long-term transient sources, the mechanisms involved are associated with complex dynamics and hydrodynamic instabilities for which there is no analytical description. However, there are many models that more or less realistically describe the emitted gravitational waves. Among the most important are Accretion disk instability (ADI) (Wang et al. 2021; Hartman et al. 2010) and Fallback accretion (FA), that can predict the emission of gravitational waves for the duration of the phenomenon, which usually lasts between 20 seconds and 2000 seconds (Fryer et al. 2002). There is also the magnetars, which produce a black hole or a supermassive neutron star that will rapidly collapse into either a black hole or a stable neutron star (Piro et al. 2017). In this case, the amplification of the magnetic field during the fusion phase leads to the appearance of a magnetar inducing a quadrupole moment, which emits gravitational waves.

3 Gamma ray bursts

Gamma-ray bursts (GRBs) are the brightest and most energetic electromagnetic events in our universe. These bursts may last from ten milliseconds to some hours. After this gamma-ray flash, the "afterglow" is emitted for a relatively long time at lower energy and longer wavelengths (X-rays, UV rays, optical, infrared IR, and radio) (Meszaros 2006).

GRBs classification GRB can be classified according to its light curve into two main parts, i) short-duration GRBs (SGRBs) and ii) long-duration GRBs (LGRBs). Events with a $T_{90} < 2$ seconds are classified as short gamma-ray bursts (T_{90} is the time required for a gamma explosion to lose 90 percent of its energy, i.e. from 5% to 95% of the accumulated photon fluence), and events with a $T_{90} > 2$ seconds are classified as long-gamma ray bursts (Kouveliotou et al. 1993).

The SGRB is often caused by the collision of a neutron star binary (NS–NS) or neutron star-black hole binary (NS-BH). Eventually, a large part of the energy is emitted in the form of GW (Berger 2014). On the other hand, most of the phenomena that produce a LGRB are the collapse of a very massive star, which eventually leads to the formation of a black hole or magnetar.

Prompt phase The defining characteristic of a gamma-ray burst is the instantaneous emission (prompt) of gamma rays, The model most often used to explain the phenomenon of gamma-ray bursts is called the fireball model. In this model, a progenitor will expel matter at ultra-relativistic speeds. Even if the fireball is not something homogeneous, this matter is composed almost entirely of electrons. Besides the fact that it must have a geometry (we are talking about jets of particles focused in our direction), the "fireball" is made up of successive layers, which travel at different speeds corresponding to Lorentz factors between 50 and 500, that is to say very close to the speed of light. When two layers come together (the fastest catching up to the other), this forms a semi-relativistic shock called internal shock and this radiation is the Prompt emission (Daigne and Mochkovitch 2002; Kumar and Zhang 2015), During the interaction between the fireball and the environment surrounding, the fireball is braked in the middle, and will begin to radiate energy at all wavelengths,

this radiation is the afterglow emission. The prompt emission takes a relatively short time, from milliseconds to minutes before the afterglow starts (Pe'Er 2015; Ryde et al. 2003; Boër et al. 2003).

Afterglow phase The afterglow is thought to arise from the external shock generated when the projectile collides with the material in the surrounding interstellar medium and is swept away by it (Meszaros 2006). When electrons are accelerated in the presence of a magnetic field, rays of different wavelengths (X-ray, optical, radio) are emitted, and this is called synchrotron emission. All GRBs are observed to have X-ray afterglows, but only about 50% of them have afterglows at optical and radio wavelengths. A GRB is called a dark burst if no afterglow is detected at optical wavelengths (Kumar and Zhang 2015).

4 National Aures Observatory

Currently, Algeria does not have any astronomical observatory that can follow scientific developments, except for the Algiers Observatory, which is located in the center of the country's capital, whose site quality is no longer sufficient for scientific goals (large light pollution), Therefore, a team of specialists (Seghouani and Boër et al.) (Seghouani et al. 2019) decided to build a new observatory, namely the National Aures Observatory NAO, capable of following the successive scientific developments. This new observatory will be a qualitative leap in the field of scientific research in Algeria, especially in that of astrophysics due to the carefully chosen location of the observatory (Seghouani et al. 2019), which will be in the Aliness site in Khenchela Governorate in the Aures mountain range east of Algeria (Seghouani 2010). This observatory will have two priorities: the first will be multi-messenger astronomy represented in the search for optical counterparts of gravitational waves (GW) and all transient astronomical phenomena such as GRB, the second priority is about early supernova search, variable stars, asteroids tracking, exoplanets, etc. For transient astronomical phenomena, some constraints must be met. One of them is that the error ellipse reaches 100°^2} degrees in the sky localization of the GW source and at the same time, the great speed with which the signal of the astronomical phenomena fades. To resolve these constraints, the RAMSES project team proposes working with a network of up to 12 or 16 robotic telescopes of 400 or 500 millimeters. Each telescope has a wide field of view FoV[1] of about 2.5°^2}, and ultra-sensitive CCD or sCMOS cameras. The speed of telescope mounts is very large, up to 80 degrees per second, and its acceleration is up to 120 deg/s^2. Each telescope will be equipped with filters that enable it to see at different wavelengths and connected to a processing system capable of analyzing images in less than 10 seconds. This group is associated with a large telescope of about 1 meter, equipped with a spectrometer and capable of tracking the target after its localization. This is the RAMSES (Robotic Advanced Multimessenger and Space Environment Surveyor) project (Figure 1), which we are

[1]The field of view is the extent of the observable world that is seen at any given moment. In the case of optical instruments or sensors, it is a solid angle through which a detector is sensitive to electromagnetic radiation.

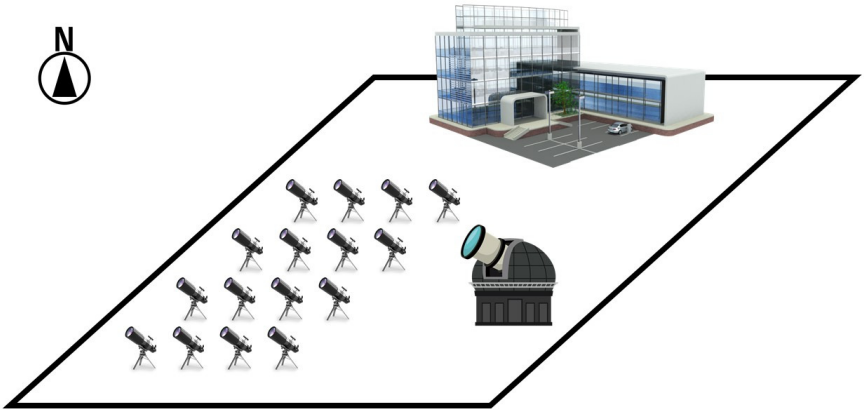


Figure 1 A simple design of The RAMSES Project. An array of 16 small telescopes associated with a large telescope equipped with a spectrometer.

Table 1 The main characteristics of the National Aures Observatory TAROT-type telescopes.

Characteristic	Telescope array
Number of telescopes	12 to 16
Optical system	Newton hyperbolic
Aperture	400 to 500 mm
Focal ration	f/3.2
Mount type	Equatorial
Axes maximum speed	80°/s
Axes maximum acceleration	120°/s^2
Maximum pointing time	1–1.5 s
Pointing precision	arcsec
Camera manufacturer	CCD or sCMOS
Images processing time	less than 10 seconds
Field of view	2.5° × 2.5°
Limiting magnitude in 10 s	18

about to simulate and exploit optimally by working to improve its scientific results (Seghouani et al. 2019).

TAROT Small telescopes are very important in the field of observing astronomical phenomena due to their high speed and are usually robotic. One of the most important robotic telescopes currently on the scene is the TAROT telescopes (Télescope à Action Rapide pour les Objets Transitoires, "Rapid-action telescope for transient objects"). The first TAROT-type telescope was designed in 1995 (Klotz et al. 2009), and it has been specifically designed for observing the visible counterpart of cosmic gamma-ray bursts (GRBs) (Boër et al. 2017). Table 1 gives some of the main characteristics of the TAROT-type telescopes that we will simulate in this work (Seghouani et al. 2019; Klotz et al. 2009; Boër et al. 2003; Boër et al. 2017).

4.1 RAMSES project as a "hunter" and "follower" of transients events

In this section we will estimate the number of transient events that RAMSES can observe, given that the limiting magnitude of the network of telescopes is $m_{lim} = 18$. The transient events that we consider are GRBs, Supernovae and Novae. The observation conditions are not taken into account.

GRBs rate estimation The probability of detecting an optical GRB event by RAMSES can be estimated by using the following formula (Greiner et al. 2011):

$$P_{GRB} = P_{swift}(1 - P_{dark})P_{m<m_{lim}}$$

P_{swift} represents the probability of GRBs being observed by Swift for all GRBs observed in the same year, which is about[2] 90%.

In our estimation, the "dark" GRB rate, denoted by the term P_{dark}, is taken to be the lower limit of 0.4 (Greiner et al. 2011).

$P_{m<m_{lim}}$ probability that the optical GRB is bright enough to be detected with a telescope having a limiting magnitude $m_{lim} = 18$. This probability, which is about 30%, is obtained using SWIFT CATALOG[3], by selecting all the events whose magnitude is less than 18 in the past five years. This means that 30 percent of the events observed in the last five years by Swift have a magnitude less than 18. Finally, knowing that about 100 GRBs are observed per year, we conclude that the RAMSES project can observe about 15 optical GRBs/year.

SNe rate estimation To get a proper estimate, we need a simulation with the following input:

a) the SN light curve and the SN rates for the different types (divided at least in Ia, Ib/c, II) as function of redshift; (b) the survey parameters: magnitude limit, field of view and cadence of the survey (how much area we cover in one day, how often we return in one field).

The output will be the number of SNe detected by the network.

However, since this is not the main purpose of our work, we can estimate very roughly this rate by considering that there are 10^{-3} SNe/square degree at $m_{lim} < 18$ at any given time in the sky. Let us assume also that the fainter SNe, which largely dominates the magnitude limited search statistics, remains at that magnitude for ten days. Therefore, if we observe the same field in two consecutive days, we find only a small fraction of new SNe (in our approximation 1/10). The number of SNe that we discover in a year are: $10^{-3} \times 365/10 \times (2.5 \times 2.5) \times N \times 100 \sim 23 \times N$ SN/year, where N is the number of telescopes and 100 is the number of field per telescope per night (Feindt et al. 2019). With $N = 16$, we find that the RAMSES Project will observe the total number of 370 SNe/yr which is not too distant from the actual discovery rate of the ASAS-SN survey[4].

Novae rate estimation With a small telescopes we can discover novae in the galaxy and in few very nearby galaxies. (Della Valle et al. 2020) report the discovery

[2]https://swift.gsfc.nasa.gov/archive/grb_table/stats/
[3]https://swift.gsfc.nasa.gov/archive/grb_table/
[4]https://www.astronomy.ohio-state.edu/asassn/index.shtml

of about 10 novae per year at a limit magnitude $m_{lim} = 18$, see also (Allen. 1954; Kopylov 1955; Sharov. 1972; Liller et al. 1987; Ciardullo et al. 1990; Van Den Bergh. 1991; Della Valle et al. 1992; Della Valle et al. 1994; Shafter. 1997; Hatano et al. 1997; Shafter et al. 2000).

5 Simulation and work method

This section is divided into two subsections. The first is a simplified explanation of the optimization method that we used in our research with some of the changes we made to fit the problem we are about to solve. The second is to project the optimization method on our problem and the steps followed to simulate the RAMSES project and the mathematical structure used.

5.1 Assignment problem using branch and bound method

5.1.1 Branch and bound method

The BB method is a generic method of solving combinatorial optimization problems. Combinatorial optimization consists in finding a point that minimizes a function, called cost, in a countable set. A naive method of solving this problem is to list all the solutions to the problem, calculate the cost for each, and then give the minimum. Sometimes it is possible to avoid listing solutions which we know, by analyzing the properties of the problem, that they are bad solutions, that is to say, solutions that cannot be the minimum.

The branch and bound method consists of enumerating these solutions intelligently by using certain properties of the problem in question. We represent the execution of the BB method through a tree structure. The root of this tree represents the set of all the solutions of the problem under consideration.

The method begins by considering the original problem with its set of solutions, called the root. Lower and upper bound procedures are applied at the root. If these two bounds are equal, then an optimal solution is found, and we stop there. Otherwise, the set of solutions is divided into two or more sub-problems, thus becoming a sub-root. The method is then applied recursively to these sub-problems, thus generating a tree structure. If an optimal solution is found for a subproblem, it is feasible, but not necessarily optimal, for the starting problem. As it can be done, it can be used to eliminate all its descendants if the lower bound of a node exceeds the value of an already known solution. Thus, one can affirm that the total optimal solution cannot be contained in the subset of the solution represented by this node. The search continues until all nodes are either explored or eliminated. For more details see (Levitin 2003).

5.1.2 Assignment problem

The assignment problem is how to best assign tasks to agents. Each agent can perform a single task for a given cost and each task must be performed by a single agent. The assignments (that is to say the agent-task pairs) all have a defined cost. The goal is to minimize the total cost of assignments to complete all tasks.

Formal definition The problem can be stated as follows. Given a set of agents S and a set of tasks T, it is possible to model the problem by a bipartite graph $G = ((S,T),\mathrm{E})$ with a function of weight on the edges $c : E \to \mathbb{R}$. E is a set of edges. The assignment problem, therefore, consists in finding a perfect matching $F \subset E$ minimizing the sum $\sum_{e\epsilon F} c(e)$ of the weights of the edges of F (Azmoodeh 1990).

Adaptation with our problem In our case, we have a network of up to 12 telescopes. At a specific moment t_0, we receive an urgent alert of an astronomical event in a certain region of the sky. We divide this region into small sections. Each telescope scans a section and the condition here is that all telescopes must arrive to their target in the shortest possible time.

From here it becomes clear that we must change the selection condition from **(the smallest total cost)** to **reduce** the **maximum individual cost** as much as possible**.** Because the cost in our case is **time,** so we choose the case in which the time of arrival of the last telescope to its place is the least possible.

5.2 RAMSES Project simulation

The National Aures Observatory consists of a network of $N\epsilon\,[6,12]$ telescopes, most of the time working on the second priority (tracking supernovas, variable stars, etc.) (Figure 2), and at a certain moment t_0 the network receives an urgent alert of the existence of an astronomical event of the first priority (GW or GRB). Telescopes abandon their current work and go to try to observe the transit astronomical phenomenon. At first, the telescopes are observing random locations in the sky, and after the urgent alert, they move to scan the error ellipse[5] that the event is supposed to be inside. The three parameters that determine the geometry of an error ellipse are the semi-major axis a, the semi-minor axis b and the angle θ between the major axis and the y-axis. Note here that the distances[6] between the initial positions of the telescopes and their targets maybe very large, up to 180 degrees.

After fixing the number N of telescopes, the simulation begins with some random choices:

1. Choose a center point for error ellipse (x_0, y_0), $x_0\epsilon\,[-180°, 180°]$ and $y_0\epsilon\,[0°, 90°]$.
2. Choose the length a and b, to determine the area of the error ellipse, $S = \pi ab$.
3. Choose the rotation angle $\theta\epsilon\,[0, \pi]$.
4. Choosing a point inside the ellipse to represent the astronomical event to be detected (x_G, y_G).
5. Choose N points from the total sky area to represent the random locations of telescopes before the alert.

After selecting these parameters randomly, which is equivalent to a simulation of the initial conditions preceding the alert, we start working on this ellipse and divide it

[5]Error ellipse is the region that contains 95% of all samples that can be drawn from the underlying Gaussian distribution. It represents an iso-contour of the Gaussian distribution, and allows you to visualize a 2D confidence interval (Wen and Chen 2010).

[6]Distance means here the angle that the telescope must rotate to move from one observation position to another.

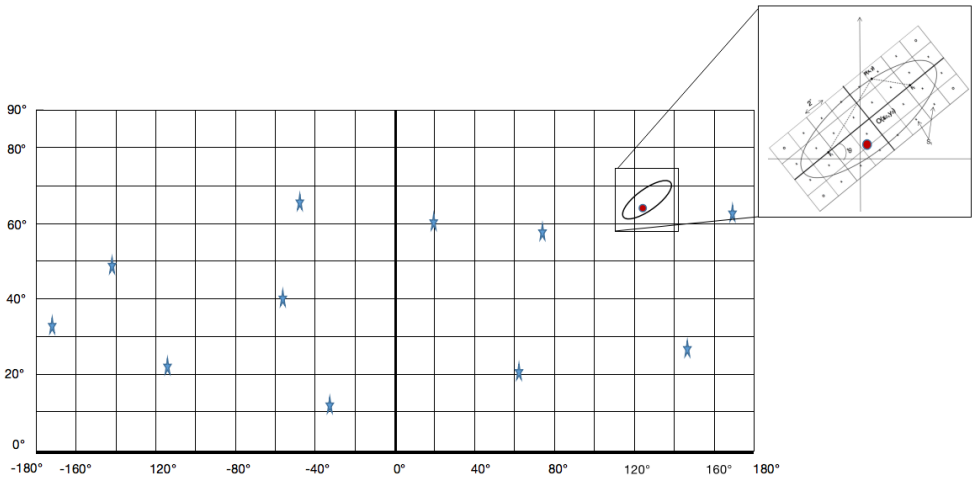


Figure 2 Representation of the sky. The blue stars represent the random locations of the telescopes before the alert, and the red dot inside the ellipse represents the astronomical event that the network of telescopes must find.

properly into small areas to be scanned by the network, and where each telescope is directed to a specific area using the BB method.

The work steps are summarized in the following:

- Divide the error region into squares suitable for TAROT's FoV.
- Find the coordinates of the two ellipse foci.
- Find the coordinates of the centers of the squares.
- Find the points inside the ellipse.
- Create a matrix whose components are the distance between the initial points of the telescopes and the points to be surveyed.
- Observation condition test (did the telescope detect the event).

After finding the final matrix and applying the BB optimization method, each telescope has its destination (coordinates where it goes to). If the event is not observed in these locations, the telescopes are redirected to new locations. Thus, they are redirected until the signal from the astronomical phenomenon is observed.

Let us now explain the previous points in detail.

5.2.1 Division of the error ellipse

To simulate the RAMSES project, the first thing we do is to work on the sky position error ellipse that we receive in the form of an urgent alert from one of the observatories that track astronomical events continuously and that are collaborating with the National Aures Observatory. This alert comes with basic parameters about the astronomical event, through which, we can plot an error ellipse to be scanned by telescopes. These parameters are the coordinates of the ellipse's center (x_0, y_0), the lengths a and b, the angle θ.

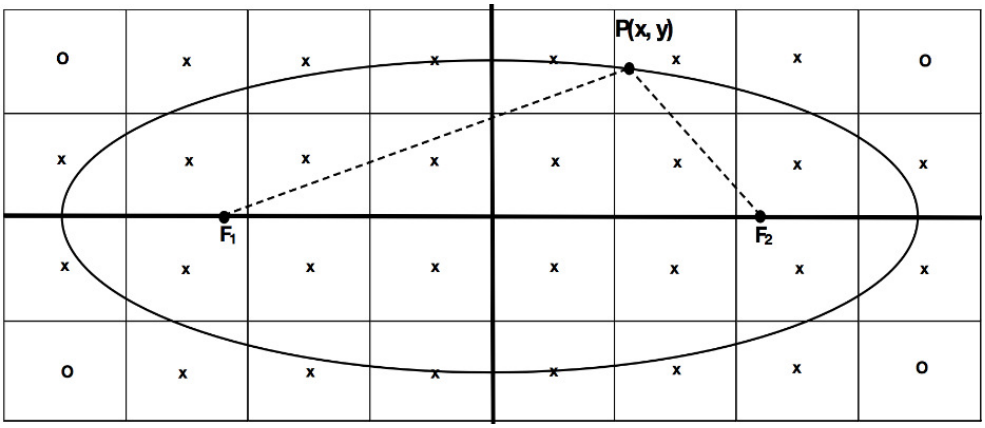


Figure 3 Method for dividing the rectangle surrounding the error ellipse. Each small square has a side length of 2 degrees. Telescopes must scan all squares inside or intersect with the ellipse.

Then we will divide this area into P small parts of a size that fits the TAROT's FoV. In our case we divide it into squares of 2° (two degrees) side length. This is done by drawing a rectangle surrounding the ellipse and dividing it into squares with a side length of 2° as shown in Figure 3. Note that the length and width of the rectangle must be a multiple of 2 so that the number of small squares is an integer.

5.2.2 Find the coordinates of the two foci and rectangular dimensions

Find the coordinates of the two foci The general equation of the ellipse (the parametric equation):

$$\begin{cases} x(t) = x_0 + a\cos\theta\cos t - b\sin\theta\sin t \\ y(t) = y_0 + a\sin\theta\cos t + b\cos\theta\sin t \end{cases} \tag{1}$$

where t is the parameter, $t\epsilon\,[0, 2\pi]$ radians, $O(x_0, y_0)$ is the ellipse's center coordinates, a and b are the semi-major and semi-minor axes respectively $(0 < b < a)$ and θ is the rotation angle, see Figure 4.

Now that the parameters a and b are known to us, finding c, which is the distance of the two foci from the center of the ellipse, is easy ($c^2 = a^2 - b^2$), and from it, we can deduce the coordinates of the two foci F_1 and F_2:

$$F_1(x_0 - c, y_0)$$
$$F_2(x_0 + c, y_0)$$

We can, then, deduce the general relationship of the coordinates of the two foci after a rotation with an angle θ, by applying the rotation matrix $R = \begin{pmatrix} \cos\theta & -\sin\theta \\ \sin\theta & \cos\theta \end{pmatrix}$,

Thus, the foci coordinates in the general case are:

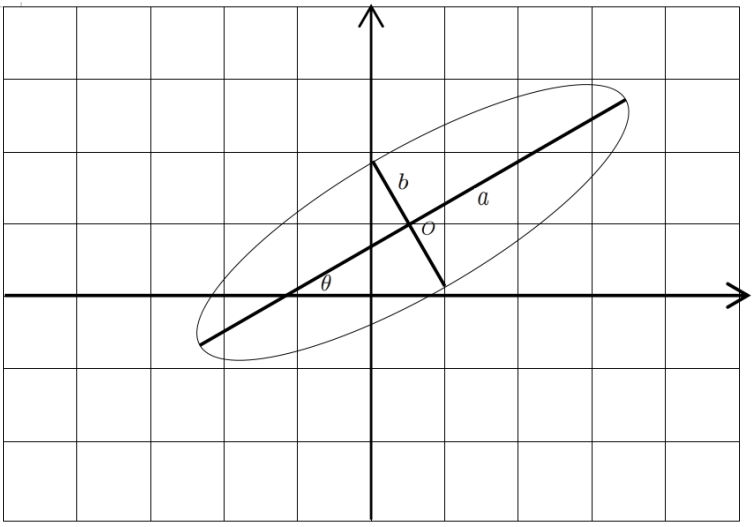


Figure 4 A representation of an ellipse in the general case, semi-major axis a and semi-minor axis b, and angle of rotation θ are shown.

$$F_1((x_0 - c)\cos\theta - y_0 \sin\theta, (x_0 - c)\sin\theta + \cos\theta)$$

$$F_2((x_0 + c)\cos\theta - y_0 \sin\theta, (x_0 + c)\sin\theta + y_0 \cos\theta)$$

Length and width of the rectangle As we divide the rectangle surrounding the error ellipse into P squares of side lengths $2°$, both length and width of the rectangle must be multiple of 2 and greater than $2a$ and $2b$, respectively.

This means that the length of the rectangle is $2{*}2\lceil a/2\rceil$ and its width is $2{*}2\lceil b/2\rceil$. Here $\lceil x\rceil$ is the ceiling function that maps x to the least integer greater than or equal to x.

5.2.3 Small squares center coordinates

After the above, we find the coordinates of the centers of the squares (see Figure 5):

$$s_{ij}(x_0 - 2\lceil a/2\rceil + 2j + 1\ , y_0 + 2\lceil b/2\rceil - 2i - 1)$$

i and j are integer numbers, with $i\epsilon[0, 2\lceil b/2\rceil - 1]$ and $j\epsilon[0, 2\lceil a/2\rceil - 1]$.

To generalize s_{ij} coordinates, we apply the rotation matrix R

$$R.s_{ij} = S_{ij} = \begin{pmatrix} (x_0 - 2\lceil a/2\rceil + 2j + 1)\cos\theta - (y_0 + 2\lceil b/2\rceil - 2i - 1)\sin\theta \\ (x_0 - 2\lceil a/2\rceil + 2j + 1)\sin\theta + (y_0 + 2\lceil b/2\rceil - 2i - 1)\cos\theta \end{pmatrix}$$

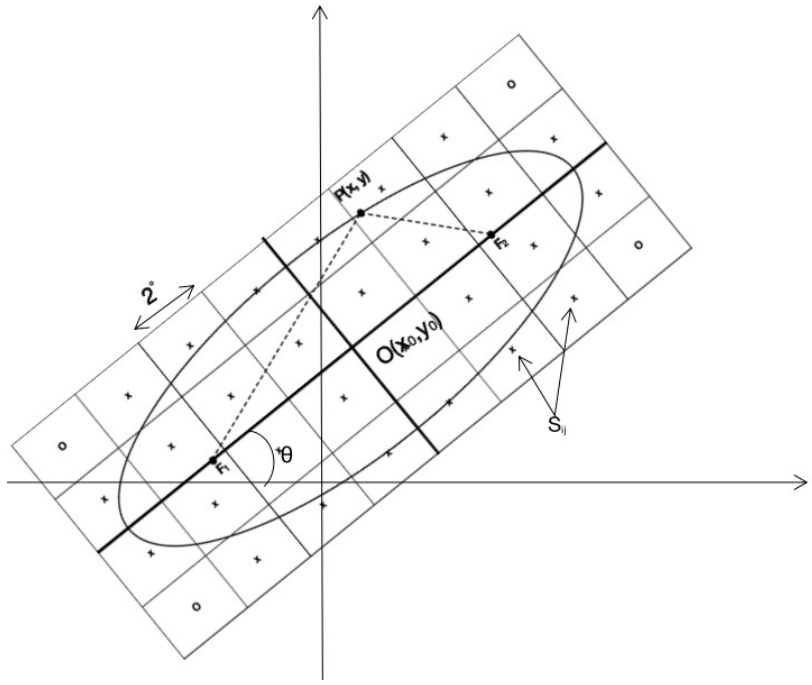


Figure 5 The general case of dividing an ellipse inside a rectangle into small squares, after a translation and a rotation by an angle θ.

5.2.4 Finding points inside the ellipse

All the area that telescopes have to scan must be inside the ellipse. This means that all points P_{ij} inside the ellipse verify the relation:

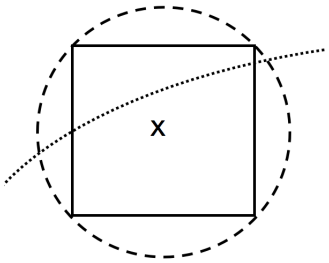
$$\|F_1P_{ij}\| + \|F_2P_{ij}\| \leq 2a$$

where $\|AB\|$ represents the distance between A and B, a is the semi-major axis.

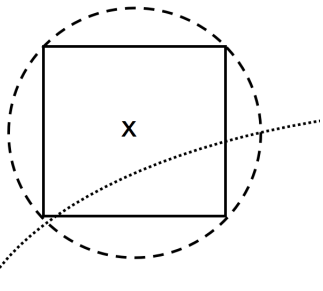
The first and second scan priority Telescopes should scan the space inside the ellipse, but since some small squares have a portion of them outside the ellipse, it would be a good idea to leave scanning them until after the squares inside the ellipse are examined.

So we have two scan priorities:

- The first priority is all squares whose center is inside the ellipse, see Figure 6a.
- The second priority is all squares whose center is outside the ellipse and has a small contribution to the error ellipse, see Figure 6b.



(a) The first scan priority.



(b) The second scan priority.

Figure 6 (a) The first priority for scanning is given to every small square whose center is inside the ellipse, whether the square is entirely inside the ellipse or most of it is inside and part of it is outside. (b) The second priority of scanning is given to every small square whose center is outside the ellipse because most of it is outside the ellipse and the probability of the event occurring in the intersection is small.

5.2.5 The cost matrix for branch and bound method

After we finished prioritizing surveys of telescopes and finding the coordinates of the small squares positions delimiting the error ellipse, we use the branch and bound method discussed in Section 5.1 to minimize the time needed to scan all these positions.

For that, we define a matrix $M$of dimensions $P \times N$, whose elements contain the time taken for each telescope T_i to reach its target position P_j. Then, we divide this matrix into several $N \times N$ small matrices M_i to apply the BB method to it.

$$M = \begin{pmatrix} M_1 \\ M_2 \\ . \\ . \\ . \\ M_i \end{pmatrix}$$

The BB method is applied to small matrices in order (because they are arranged in order of priority), each array simulating the process of pointing telescopes to scan

specific small areas within the error ellipse. We should emphasize here that we are applying the BB method to optimize the time required for all telescopes to reach their positions as quickly as possible.

5.2.6 Observation condition test

After assigning each telescope to survey a specific area, the telescope is considered to have observed the astronomical event if the distance between the point representing the astronomical event (x_G, y_G) and the location to which the telescope was directed to is less than or equal to $\sqrt{2}$, see Figure 7.

For real telescopes, it takes time to process the image to verify the presence of the source or not. For the National Aures Observatory the image processing time will be less than 10 seconds (Seghouani et al. 2019), and we should take it into account in our simulation.

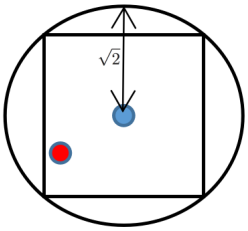


Figure 7 In the simulation process, to observe the event, the distance between the center of the square (represented in blue) and the point representing the event (x_G, y_G) (represented in red) must be less than $\sqrt{2}$. That is, the event position should be within the circle of FoV.

If the event is not observed after the first pointing of the telescopes, the telescopes are re-pointed with a new matrix whose values are the time taken by the telescope T_i to reach the new position P_j. This process is repeated until the astronomical event is observed and the observing telescope is known (Figure 8).

By knowing the distance D from the starting point to the target point of each telescope and by knowing the speed of rotation v and acceleration a of the telescopes, see Table 2, we can calculate the time it takes for each telescope to move from one position to another. By knowing also the number of orientation times O needed, we can estimate the total time t from starting the survey to observing the event.

$$t = \sum_{i=1}^{O} \left\{ \left(\sqrt{\frac{D_i}{a}} \right) \Theta(2x_0\text{-D}) + \left(\sqrt{\frac{2x_0}{a}} + \frac{D_i - 2x_0}{\text{v}} \right) \Theta(\text{D-}2x_0) - \left(\sqrt{\frac{D_i}{a}} \right) \delta(2x_0\text{-}D_i) \right\} \tag{2}$$

where x_0 is the distance traveled by the telescope before reaching its maximum speed, Θ is the Heaviside step function, and δ is Kronecker delta function[7].

[7] $\delta(2x_0 - D_i) = \begin{cases} 1 & \text{if } 2x_0 = D_i \\ 0 & \text{if } 2x_0 \neq D_i \end{cases}$

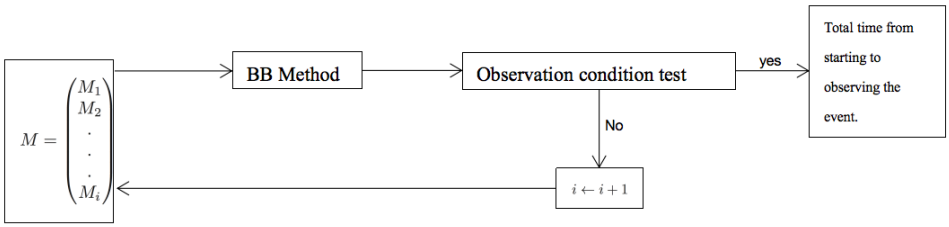


Figure 8 A diagram showing how the simulation works. From dividing the matrix M, then applying the BB method and finally finding the total time from starting the search to observing the event.

Table 2 The table shows the main characteristics of the National Aures Observatory used in the simulation.

Characteristic	Telescope array
Number of telescopes	6 to 12
Axes maximum speed	$80^\circ/\text{s}$
Axes maximum acceleration	$120^\circ/\text{s}^2$
Images processing time	10 seconds
Field of view	$2.5^\circ \times 2.5^\circ$

After completing the method and finding the time required for the set of N telescopes to observe the event, we repeat this simulation process 10,000 times to make a comprehensive statistical study.

Note that for this work we change the number of telescopes used ($N = 6$, $N = 7$, $N = 8$, $N = 9$, $N = 10$, $N = 11$, $N = 12$), in order to study the effect of the number of telescopes on the time required for observation and change the area of the error ellipse to be scanned from 30 to 140°^2} for studying the effect of the area to be surveyed on the number of telescopes needed. Our results are shown in the next section.

6 Results and discussion

In this research, which is a simulation of the future RAMSES project (Seghouani et al. 2019), we used the branch and bound optimization method to: i) improve the time required for the network of telescopes to find the source signal of the astronomical phenomenon, taking into account the number of telescopes used, ii) study the efficiency of telescopes every time they are redirected, and iii) study the effect of the area to be surveyed on the number of telescopes needed.

We obtained the results after writing an integrated simulation program based on the characteristics we have about this robotic network (speed, acceleration, field of view, image processing time,...) and the astrophysical phenomena it studies, taken from (Seghouani et al. 2019). These results indicate the following:

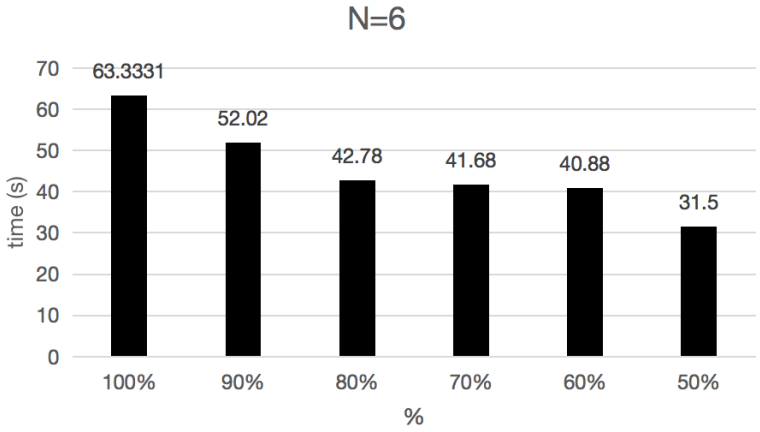


Figure 9 The histogram represents the time required for 6 telescopes to observe the event. Each column represents the time required for the best cases to observe the event.

i) The effect of the number of telescopes used on the time required to observe the event. For $N = 6$, see Figure 9, results show that we can observe the signal source 63.33 seconds after the alert, using only 6 telescopes. This means that we can use half of the RAMSES network to get results in about a minute, which is presented as a challenge in (Seghouani et al. 2019), and that with 100% reliability (meaning that all of the 10,000 simulations took 63.33 seconds or less to detect the signal).

But if we talk about the best 80% of cases**,** these six telescopes were able to pick up the signal 42.78 seconds after the alert. And 50% of the cases were able to pick up the signal in about half a minute, 31.5 seconds. This indicates the great efficiency of the method of improving the time taken to pick up the signal, even if we use only half the number of available telescopes.

All of the obtained data (from $N = 6$ to $N = 12$) are shown in the histograms of Appendix A1.

ii) The efficiency of telescopes every time they are redirected. Now from another point of view, which is the efficiency of telescopes every time they are redirected, we note that the number of orientations does not exceed 6 times even if only 6 telescopes are used.

First pointing: represented in blue in Figure 10. For the first pointing, where telescopes from their random location are directed into a small target area within the error ellipse to track the event, 42.04% of the cases were able to catch the signal when we used 12 telescopes, while when using 11 telescopes 39.43% of the cases were able to detect the event immediately after this first positioning. For the use of 10 telescopes, 30.76% of the cases were able to complete successfully the monitoring task in the first step. Finally, as expected, this percentage will decrease as the number of telescopes decreases until it reaches 16.82% when using only 6 telescopes.

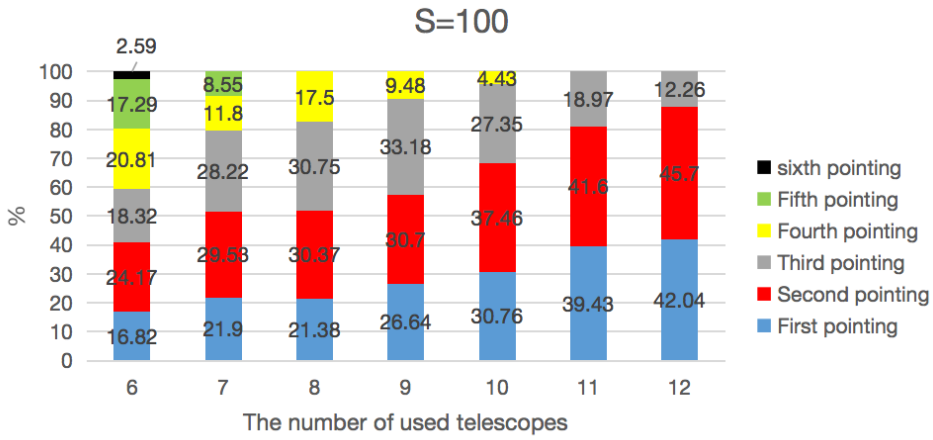


Figure 10 The efficiency of telescopes every time they are redirected for scanning an error ellipse of 100°^2}, each color represents a transition from one position to the next.

iii) The effect of the area to be surveyed on the number of telescopes needed The areas to be surveyed by the RAMSES project could be relatively small ones as those that usually come from urgent alerts sent by gamma-ray tracking satellites such as "Swift" (the area of error could be about 30 square degrees) (Abbott et al. 2017). or relatively large areas, as those sent by gravitational wave observatories (error area within 100 square degrees and more).

To study the effect of the area to be surveyed on the number of telescopes needed, we change the area S to be scanned from 30 to 140°^2}, and, for each fixed value of S, we study the effectiveness of telescopes from $N = 6$ to $N = 12$. The results are as follows:

For S=30: In the case of studying small areas, a group of telescopes may be enough to cover the entire area, so the event will be observed immediately after directing the telescopes, see Figure 11. In the case of an area of 30 square degrees, 9 telescopes are enough to observe the event directly after the first orientation. In the same conditions, 8 telescopes are enough to observe the event, with a rate of 89.4%. While 6 telescopes can observe the event in their first pointing with a percentage of 61.8%, and they need a second pointing to achieve their task in all cases.

For S=110: As seen previously, the area of error ellipse that comes from GW observatories such as LIGO and Virgo is large compared to the error ellipses sent by satellites that monitor the optical part associated with gravitational waves such as Swift, In the case of $S = 110^{\circ^2}$, see Figure 12, a network of 12 telescopes can observe the event in all cases after three steps. The event was detected after a first pointing in 40.3% of cases, while the second pointing allows a detection in 35.5% of cases. A network of 10 telescopes needs 4 successive orientations of the telescopes, whereas a network of 6 telescopes needs 6 successive orientations to complete successfully the observation in all cases.

All of the obtained data (from S=30 to S=140) are shown in the histograms of Appendix A2.

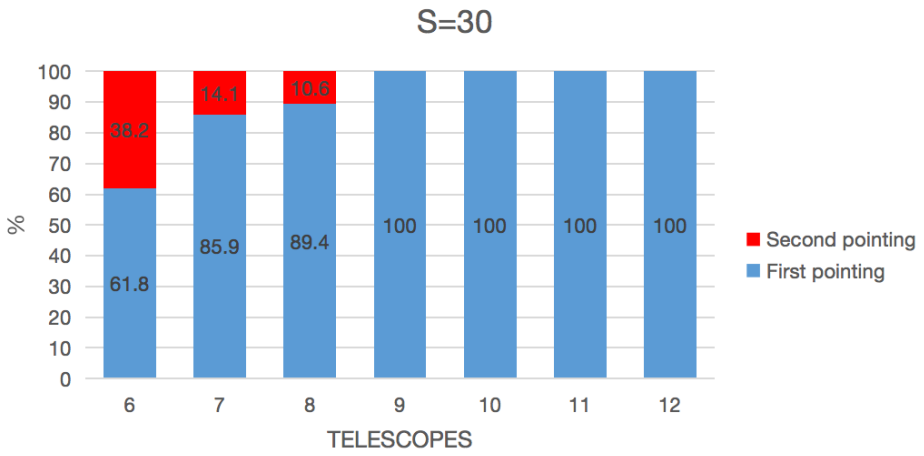


Figure 11 The histogram represents the effect of the number of telescopes used on the number of re-pointing needed to observe the event in an error ellipse of 30°^2}. The blue color represents the first direction to the error area, the red color represents the second direction.

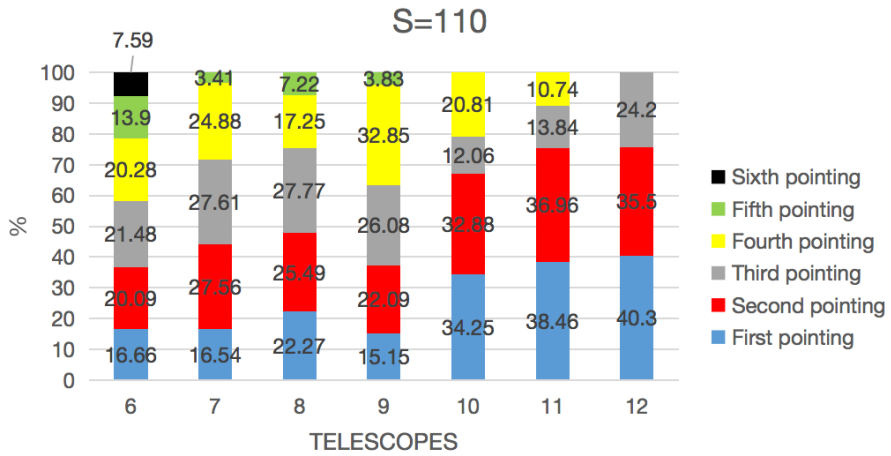


Figure 12 The histogram represents the effect of the number of telescopes used on the number of re-pointing needed to observe the event in an error ellipse of 110°^2}.

Number of telescopes needed for an observation after knowing the area to be surveyed Through the results we obtained, which are shown in Appendix A2, we will set the number of telescopes needed for each area to be successfully scanned in less than 40 seconds. The results about 100% chance of detection are shown in Table 3, and for 80% chance of detection, they are shown in Table 4.

Table 3 The number of telescopes needed to scan the error ellipse and monitor successfully the event in a period not exceeding 40 seconds with a 100% chance of detection.

Areas S to be scanned, in square degrees	Number of telescopes needed
Less than or equal to 70	6
$70 < S \leq 90$	7
$90 < S \leq 100$	8
$100 < S \leq 120$	9
$120 < S \leq 130$	11
$130 < S \leq 140$	12

Table 4 The number of telescopes needed to scan the error ellipse and monitor successfully the event in a period not exceeding 40 seconds with an 80% chance of detection.

Areas S to be scanned, in square degrees	Number of telescopes needed
Less than or equal to 110	6
$110 < S \leq 130$	7
$130 < S \leq 140$	8

7 Conclusion

In conclusion, this study revolves around the use of optimization methods to reduce the time required to scan sky position error ellipses of astronomical events that will be sent by multi-messenger surveyors, like gamma-ray tracking satellites or gravitational wave observatories, by a TAROT-type telescopes network.

The importance of this study is that it simulates a network of telescopes under construction, through which we can exploit it optimally, by finding ways to improve the time taken to observe an astronomical event (the least possible), and reduce the number of used telescopes sufficient to monitor the astronomical event in the shortest possible time after the alert.

Additionally we studied the effect of the number of telescopes on the speed of observation, and the effectiveness of telescopes in finding the source, every time they are redirected, is analysed. Moreover we saw that by using half of the National Aures Observatory network, we can monitor successfully the astronomical event in one minute, while the time required for 12 telescopes to discover the source does not exceed half a minute. Furthermore, a network of 12 telescopes can pick up the source signal from the first positioning step in 42% of cases.

By investigating the effect of the area to be surveyed on the number of telescopes needed, we were able to propose a statistical method through which we can know the number of telescopes to be dedicated in order to monitor successfully the event in a specific area, which guarantees an optimal use of the observatory.

Moreover, the fastest reaction to an alert coming from a Swift is in the range of 140 s, while the typical time for nighttime bursts is in the range of 200–300 s (Greiner et al. 2011), while we were able to reduce this time to just 40 seconds using this network of telescopes.

Therefore, these are important findings, especially for studying the prompt emission and early afterglow of gamma-ray bursts associated with gravitational waves, and we can easily generalize this study to include any other network of telescopes whose main features are known such as speed, acceleration and field of view.

References

Aasi, J.; Abbott, B.P.; Abbott, R.; et al. (2015). Advanced ligo. CQGra, 32(7): 074001.

Abbott, B.P.; Abbott, R.; Abbott, T.D.; et al. (2016). Observation of gravitational waves from a binary black hole merger. PhRvL, 116(6):061102.

Abbott, B.P.; Abbott, R.; Abbott, T.D.; et al. (2017). Multi-messenger observations of a binary neutron star merger. ApJ, 848(2):L12.

Allen, C. W. (1954). Whole-sky statistics of celestial objects. MNRAS, 114(4), 387-405.

Azmoodeh, M. (1990). Abstract data types and algorithms. Springer.

Beckman, J.E. (2021). Multimessenger astronomy. ISBN: 978-3-030-68372-6. Cham: Springer International Publishing.

Berger, E. (2014). Short-duration gamma-ray bursts. ARA&A, 52:43–105.

Boër, M.; Klotz, A.; Atteia, J.L. ; et al. (2003). The gamma-ray burst hunt at la silla the tarot-s very fast moving telescope. Msngr, 113:45–48.

Boër, M.; Klotz, A.; Laugier, R.; et al. (2017). Tarot: a network for space surveillance and tracking operations. In 7th European Conference on Space Debris ESA/ESOC, Darmstadt/Germany.

Branchesi, M. (2016). Multi-messenger astronomy: gravitational waves, neutrinos, photons, and cosmic rays. In Journal of Physics: Conference Series, volume 718, page 022004. IOP Publishing.

Camp, J.; Barthelmy, S.; Blackburn, L.; et al. (2013). Using iss telescopes for electromagnetic follow-up of gravitational wave detections of ns-ns and ns-bh mergers. ExA, 36(3):505–522.

Ciardullo, R.; Ford, H. C.; Williams, R. E.; et al. (1990). The nova rate in the elliptical component of NGC 5128. AJ, 99, 1079-1087.

Coulter, D.A.; Foley, R.J.; Kilpatrick, C.D.; et al. (2017). Swope supernova survey 2017a (sss17a), the optical counterpart to a gravitational wave source. Sci, 358(6370):1556–1558.

Daigne, F.; Mochkovitch, R. (2002). The expected thermal precursors of gamma-ray bursts in the internal shock model. MNRAS, 336(4):1271–1280.

Della Valle, M.; Bianchini, A.; Livio, M.;et al. (1992). On the possible existence of two classes of progenitors for classical novae. A&A, 266, 232-236.

Della Valle; M.; Livio, M. (1994). On the nova rate in the Galaxy. A&A, 286, 786-788.

Della Valle, M.; Izzo, L. (2020). Observations of galactic and extragalactic novae. A&ARV, 28(1), 1-118.

Einstein, A.; et al. (1905). On the electrodynamics of moving bodies. AnP, 17(10): 891–921.

Feindt, U.; Nordin, J.; Rigault, M.; et al. (2019). simsurvey: estimating transient discovery rates for the Zwicky transient facility. JCAP, 2019(10), 005.

Frey, V. (2018). Recherche de signaux d'ondes gravitationnelles transitoires de longue durée avec les données des détecteurs advanced Virgo et advanced LIGO. PhD thesis, Université Paris-Saclay.

Fryer, C.L.; Holz, D.E.; Hughes, S.A. (2002). Gravitational wave emission from core collapse of massive stars. ApJ, 565(1):430.

Greiner, J.; Krühler, T.; Klose, S.; et al. (2011). The nature of "dark" gamma-ray bursts. A&A, 526, A30.

Hartman, J.M.; Galloway, D.K.; Chakrabarty, D. (2010). A double outburst from igrj00291+ 5934: implications for accretion disk instability theory. ApJ, 726(1):26.

Hatano, K.; Branch, D.; Fisher, A.; et al. (1997). On the spatial distribution and occurrence rate of Galactic classical novae. MNRAS, 290(1), 113-118.

Klotz, A.; Boër, M.; Atteia, J. L.; et al. (2009). Early optical observations of gamma-ray bursts by the tarot telescopes: Period 2001-2008. ApJ, 137(5):4100.

Kopylov, I. M. (1955). Comparison of morphological properties and spatial distribution of novae and supernovae. BCrAO, 15, 140-146.

Kouveliotou, C.; Meegan, C.A.; Fishman, G.J.; et al. (1993). Identification of two classes of gamma-ray bursts. ApJ, 413:L101–L104.

Kumar, P.; Zhang, B. (2015). The physics of gamma-ray bursts & relativistic jets. PhR, 561:1–109.

Levitin, A. (2003). Introduction to the design and analysis of algorithms addison-wesley. Boston, MA.

Lorentz, H. A. (1899). Considerations on gravitation. KNAB, 2:559–574.

Meszaros, P. (2006). Gamma-ray bursts. RPPh, 69(8):2259.

Pe'er, A. (2015). Physics of gamma-ray bursts prompt emission. AdAst, 2015.

Liller, W.; Mayer, B. (1987). The rate of nova production in the galaxy. PASP, 99(617), 606.

Pirani, F.A.E. (1956). On the physical significance of the riemann tensor. AcPP, 15:389–405.

Piro, A.L.; Giacomazzo, B.; Perna, R. (2017). The fate of neutron star binary mergers. ApJ, 844(2):L19.

Poincaré, H. (1905). La dynamique de l'électron par Henri Poincaré (The dynamics of the electron by Henri Poincaré).

Rollins, J. G. (2011). Multimessenger astronomy with low-latency searches for transient gravitational waves. Columbia University.

Ryde, F.; Borgonovo, L.; Larsson, S.; et al. (2003). Gamma-ray bursts observed by the integral-spi anticoincidence shield: A study of individual pulses and temporal variability. A&A, 411(1):L331–L342.

Seghouani, N. (2010). Un Observatoire dans la région des Aurès. AfrSK, 14:44.

Seghouani, N.; Boër, M.; Mimouni, J. (2019). National aures observatory: A new multimessenger facility. JPhCo, 1269(012001). IOP Publishing.

Shafter, A. W. (1997). On the nova rate in the galaxy. ApJ, 487(1), 226.

Shafter, A. W.; Ciardullo, R.; Pritchet, C. J. (2000). Novae in external galaxies: M51, M87, and M101. ApJ, 530(1), 193.

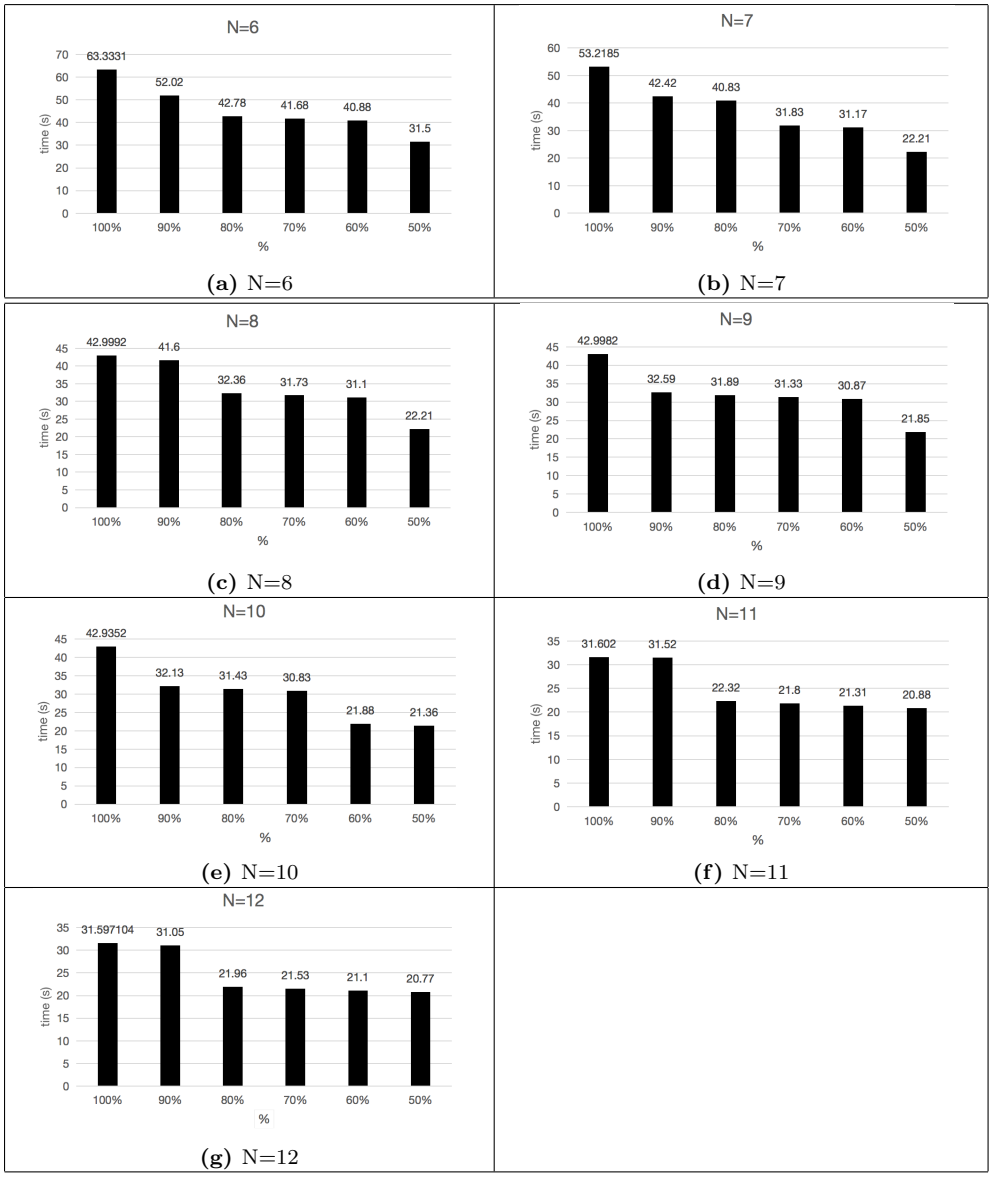
Sharov, A. S. (1972). Estimate for the Frequency of Novae in the Andromeda Nebula and our Galaxy. SvA, 16, 41.

Van Den Bergh, S. (1991). Supernova rates: A progress report. PhR, 204(6), 385-400.

Wang, M.; Chen, S.; Jing, J. (2021). Effect of gravitational wave on shadow of a schwarzschild black hole. EPJC, 81(6):1–13.
Wen, L.; Chen, Y. (2010). Geometrical expression for the angular resolution of a network of gravitational-wave detectors. PhRvD, 81(8):082001.

Appendix A1

Here we show our results about the effect of the number of telescopes used ($N = 6$ to $N = 12$) on the time required to observe the event. Each column in the histograms represents the time required for the best cases to observe the event.



(a) N=6 **(b)** N=7

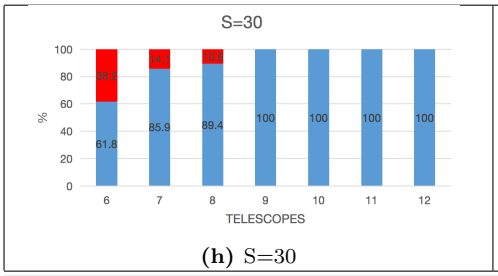
(c) N=8 **(d)** N=9

(e) N=10 **(f)** N=11

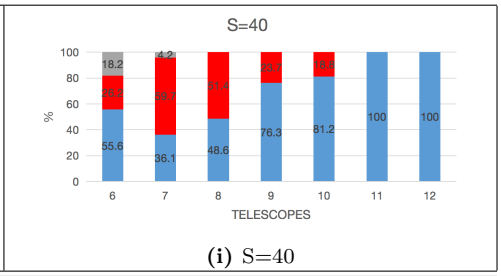
(g) N=12

Appendix A2

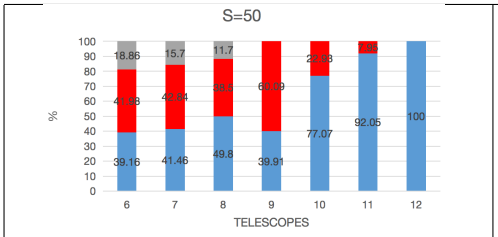
Here we show our results about the study of the number of telescopes needed for an observation after knowing the area to be surveyed. The area to be scanned by the telescopes is varying from 30 to 140. Every time we change the number of used telescopes (from 6 to 12), we repeat the simulation 10,000 times. Each color represents the probability of detecting the event, for example, the blue color represents the probability of detecting the event immediately after the first pointing, the red color represents the same probability after the second pointing, ... etc.



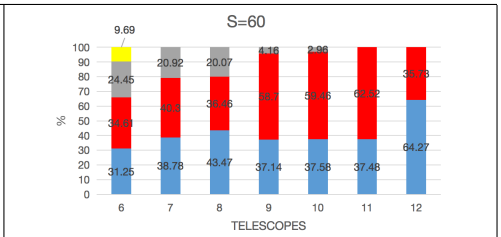
(h) S=30



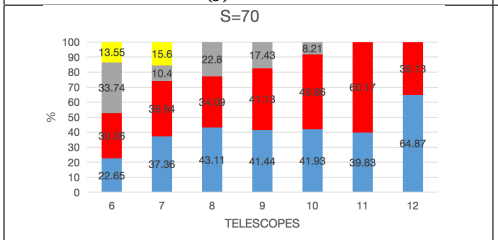
(i) S=40



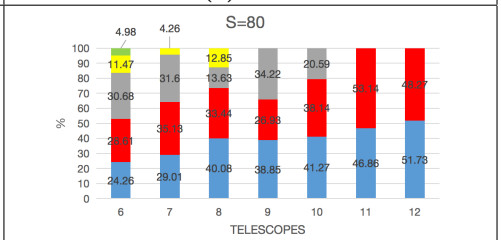
(j) S=50



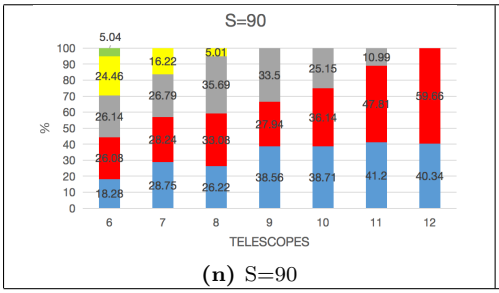
(k) S=60



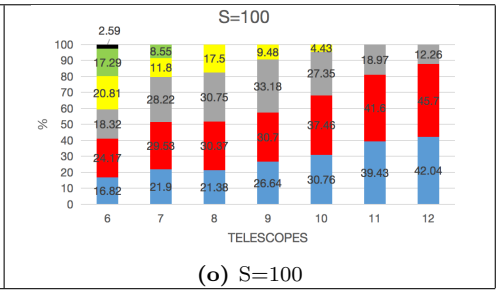
(l) S=70



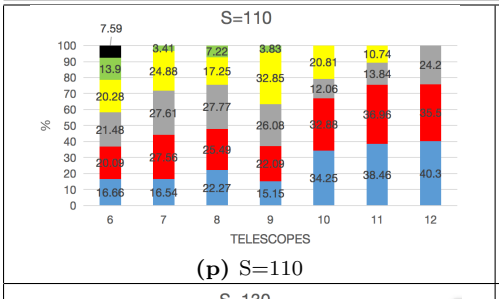
(m) S=80



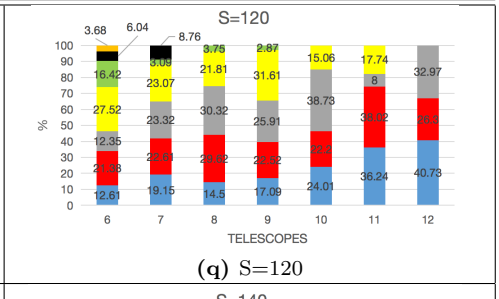
(n) S=90



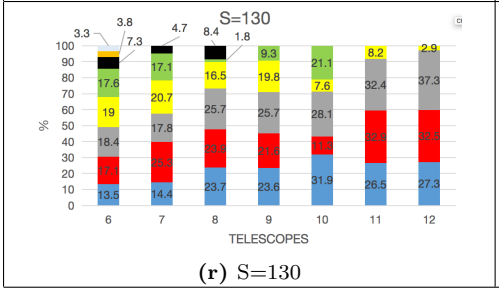
(o) S=100



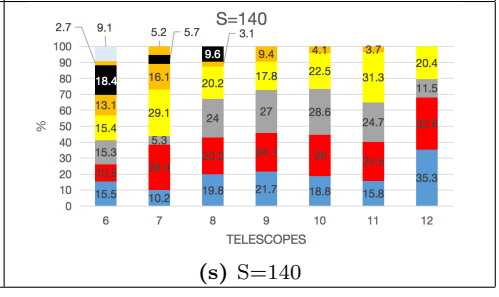
(p) S=110



(q) S=120



(r) S=130



(s) S=140